TECHNICAL MEMORANDUM

324

A fast radiative transfer model for simulation of IASI radiances

M. Matricardi and R. Saunders

Research Department

December 2000

European Centre for Medium-Range Weather Forecasts
Europäisches Zentrum für mittelfristige Wettervorhersage
Centre européen pour les prévisions météorologiques à moyen

Abstract

A fast radiative transfer model has been developed for pre-launch simulation studies of IASI data and for the exploitation of IASI radiances within the framework of an NWP variational analysis scheme. The model uses profile dependent predictors to parameterize the atmospheric optical depths and is fast enough to cope with the processing of observations in near real time and with the several thousands of transmittance calculations required to simulate radiances from a full range of atmospheric conditions. The development of the model has involved the selection of a training set of atmospheric profiles, the production of a line-by-line transmittance database, the selection of optimal predictors for the gases considered in the study and the production of regression coefficients for the fast transmittance scheme. The model fit to the line-by-line radiances shows that it can reproduce the line-by-line radiances to a degree of accuracy that is at or below the instrumental noise.

1. INTRODUCTION

One of the primary needs of operational Numerical Weather Prediction (NWP) centres and an important aim of the World Climate Research Programme (WCRP) is to improve our understanding of the atmospheric and surface hydrological cycle [Global Energy and Water Cycle Experiment (GEWEX) science plan [1]]. This is a pre-requisite for making improvements in NWP models. Another requirement of the climate change community is to monitor the concentrations of the atmospheric minor constituents consistently over a long period of time.

One step forward in these objectives will be the availability of high resolution infrared sounder data on operational meteorological polar orbiters which will provide temperature and constituent profiles at a higher accuracy and with more vertical resolution than the existing filter wheel radiometers. The Infrared Atmospheric Sounding Interferometer (IASI) has been designed as an advanced infrared sounder on the next generation of operational meteorological polar orbiters. In combination with the Advanced Microwave Sounding Unit (AMSU-A), the Microwave Humidity Sounder (MHS), and the Advanced Very High Resolution Radiometer (AVHRR/3), this is the core payload of the European Organisation for Exploitation of Meteorological Satellites (EUMETSAT) Meteorological Operational Satellite (METOP-1) and will contribute to the primary mission objective of METOP-1 that is the measurement of meteorological parameters for NWP and climate models.

The IASI instrument is a Fourier-Transform Spectrometer (FTS). The design of the interferometer is based on a classical Michelson instrument with a -2 to +2 cm optical path difference (OPD) range. IASI has a constant spectral sampling interval of 0.25 cm^{-1} and it will cover the spectral range from the CH_4 absorption band at 3.62 μm (2760 cm^{-1}) to the CO_2 absorption band at 15.5 μm (645 cm^{-1}) with an unapodized spectral resolution between 0.35 and 0.5 cm^{-1}. IASI measures from a polar orbit the spectrum of infrared radiation emitted by the Earth's atmosphere and surface with the objective of providing improved tropospheric soundings of temperature, moisture and some minor constituents, and documenting the radiative spectral properties of surfaces and clouds. The IASI spectral range is divided into three bands ranging from 645 to 1210 cm^{-1}, (band one), from 1210 to 2000 cm^{-1}, (band two), and from 2000 to 2760 cm^{-1}, (band three). Band one will be primarily used for temperature and ozone sounding, band two for water vapour sounding and for the retrieval of N_2O and CH_4 column amounts while band three will be used for temperature sounding and for the retrieval of N_2O and CO column amounts. In particular the IASI system is expected to provide information on the profiles of temperature in the free troposphere and lower stratosphere with an accuracy of 1 K and vertical resolution of 1 km. Profiles of water

vapour in the free troposphere and lower stratosphere are expected to be inferred with an accuracy of 10% in relative humidity and vertical resolution of 1 to 2 km in the low troposphere.

Given the potential benefits of IASI for NWP, preparations are being made at the European Centre for Medium-Range Weather Forecasts (ECMWF) for exploiting the IASI datasets. In recent years ECMWF has moved from using retrieved temperature and humidity profiles from the Television InfraRed Observation Satellite (TIROS-N) Operational Vertical Sounder (TOVS)[2] to assimilating the radiances directly into the model using a variational analysis scheme, for example 1D-Var described by Eyre et al.[3] for a single profile retrieval or 4D-Var described by Rabier et al.[4] for a global NWP analysis. A prerequisite for exploiting the IASI radiance data in the NWP model using the variational analysis scheme is the development of a fast radiative transfer (RT) model to accurately predict IASI radiances given first guess model fields of temperature, water vapour, ozone, surface emissivity and perhaps later cloud. This fast RT model has to simulate part or all of the IASI radiance spectrum for each observation point to give the model equivalent of the observation with which the measurement is compared. The fast RT model is also required for pre-launch studies to predict the range of radiances the instrument will measure. It must be fast enough to cope with the processing of observations in near real-time and with the several thousands of transmittance calculations required to simulate radiances from a full range of atmospheric conditions.

ECMWF uses operationally the clear radiances from the TIROS-N Operational Vertical Sounder (TOVS). The model used to process data from the High-resolution Infra-red Radiation Sounder (HIRS) and the Advanced Microwave Sounding Unit (AMSU) carried on the National Oceanic and Atmospheric Administration (NOAA) polar orbiting satellite is the Radiative Transfer for Tiros Operational Vertical Sounder (RTTOV) [5]

The fast RT model developed at ECMWF for exploiting IASI radiances is based on the approach followed by RTTOV. It contains a fast model of the transmittances of the atmospheric gases that is generated from accurate line-by-line transmittances for a set of diverse atmospheric profiles over the IASI wavenumber range. The monochromatic transmittances are convolved with the appropriate IASI Instrument Spectral Response Function (ISRF) and used to compute channel-specific regression coefficients by using a selected set of predictors. These regression coefficients can then be used by the fast transmittance model to compute transmittances given any other input profile. This parametrization of the transmittances makes the model computationally efficient and in principle should not add significantly to the errors generated by uncertainties in the spectroscopic data used by the line-by-line model. The RTTOV approach is used operationally at several NWP centres. A different approach known as the Optical Path Transmittance (OPTRAN) method has been developed recently (McMillin et al.[6], McMillin et al.[7]) and implemented at the National Center for Environmental Prediction (NCEP).

This paper deals with the methods that were applied to develop RTIASI, the ECMWF fast RT model for IASI. It has involved the formulation of the radiative transfer model (section 2), the selection of a new training set of atmospheric profiles (section 3), the production of a line-by-line transmittance database (section 4), the selection of optimal predictors and the production of regression coefficients for the fast transmittance scheme (section 5). Section 6 describes results of a comparison of radiances computed with the line-by-line transmittances and with the fast RT model for a dependent and an independent set of profiles respectively. Conclusions are given in section 7.

2. THE FORMULATION OF THE RADIATIVE TRANSFER MODEL

The current formulation of RTIASI, assumes that for a plane-parallel atmosphere in local thermodynamic equilibrium with no scattering, the upwelling radiance at the top of the atmosphere can be written as [8]

$$R(\tilde{\nu},\theta) = (1-N)R^{clr}(\tilde{\nu},\theta) + NR^{cld}(\tilde{\nu},\theta) \tag{1}$$

where $R^{clr}(\tilde{\nu},\theta)$ and $R^{cld}(\tilde{\nu},\theta)$ are the clear-column and overcast radiances at wavenumber $\tilde{\nu}$ and zenith angle θ and N is the fractional cloud cover assumed here to be in a single layer with unit cloud top emissivity. If we assume specular reflection at the Earth's surface, the monochromatic clear-column radiance can be written as (Goody et al.[9]):

$$R^{clr}(\tilde{\nu},\theta) = \tau_s(\tilde{\nu},\theta)\varepsilon_s(\tilde{\nu},\theta)B(\tilde{\nu},T_s) + \int_{\tau_s}^{1} B(\tilde{\nu},T)d\tau + [1-\varepsilon_s(\tilde{\nu},\theta)]\tau_s^2(\tilde{\nu},\theta)\int_{\tau_s}^{1}(B(\tilde{\nu},T)/\tau^2)d\tau \tag{2}$$

where $B(\tilde{\nu},T)$ is the Planck function for a scene temperature T, τ is the atmospheric level to space transmittance and $\varepsilon_s(\tilde{\nu},\theta)$ is the surface emissivity; the subscript "s" refers here to the surface. Note that the first and third terms on the right hand side of eq. (2) are the radiance from the surface and the second term is the radiance emitted by the atmosphere. In particular the third term is the thermal radiance reflected from the surface. It is important to include the reflected thermal radiance in eq. (2) because a proper treatment of this term helps separate surface temperature from surface emissivity. $R^{cld}(\tilde{\nu},\theta)$ is defined as:

$$R^{cld}(\tilde{\nu},\theta) = \tau_{cld}(\tilde{\nu},\theta)B(\tilde{\nu},T_{cld}) + \int_{\tau_{cld}}^{1} B(\tilde{\nu},T)d\tau \tag{3}$$

where $\tau_{cld}(\tilde{\nu},\theta)$ is the cloud top to space transmittance, and T_{cld} is the cloud top temperature. To represent the outgoing radiance as viewed by IASI, the spectrum of monochromatic radiance given by eq. (1) must be convolved with the appropriate ISRF. One usually write

$$\hat{R}(\tilde{\nu}^*,\theta) = \int_{-\infty}^{+\infty} R(\tilde{\nu},\theta)\, f(\tilde{\nu}^* - \tilde{\nu})\, d\tilde{\nu} \tag{4}$$

where $f(\tilde{\nu}^* - \nu)$ is the normalized ISRF and ^ over the symbol denotes convolution. Here $\tilde{\nu}^*$ is the central wavenumber of the IASI channel. The monochromatic radiance $R(\tilde{\nu},\theta)$ can be accurately computed by a line-by-line model but the whole process of calculating and convolving the monochromatic radiance is too time consuming to be performed in real time. In this paper we follow the approach of computing approximate convolved radiances assuming that eq. (1) can be applied to the spectrally-averaged radiance and the spectrally-averaged transmittance. The radiance calculation is performed assuming the atmosphere is subdivided into a number of homogeneous layers of fixed pressure. We can rewrite eq. (1) in discrete layer notation for L

atmospheric layers (the atmospheric layers are numbered from space, layer 1, to the first layer above the surface, layer L) and for a single viewing angle to simplify the notation:

$$\hat{R}_{\tilde{\nu}^*}^{clr} = \hat{\tau}_{s,\tilde{\nu}^*}\, \varepsilon_{s,\tilde{\nu}^*}\, B_{\tilde{\nu}^*}(T_s) + \left(\sum_{j=1}^{L} \hat{R}_{j,\tilde{\nu}^*}^{u} \right) + (1 - \varepsilon_{s,\tilde{\nu}^*}) \times \left[\sum_{j=1}^{L} \hat{R}_{j,\tilde{\nu}^*}^{u} \left(\hat{\tau}_{s,\tilde{\nu}^*}^2 / \hat{\tau}_{s,\tilde{\nu}^*}^2\, \hat{\tau}_{j-1,\tilde{\nu}^*}^2 \right) \right] + \hat{R}_{\tilde{\nu}^*}^{/} \qquad (5)$$

where $\hat{\tau}_{j,\tilde{\nu}^*}$ is the convolved transmittance from a given presssure level p_j to space and $\hat{R}_{j,\tilde{\nu}^*}^{u}$ is defined as:

$$\hat{R}_{j,\tilde{\nu}^*}^{u} = B_{\tilde{\nu}^*}(T_j)(\hat{\tau}_{j-1,\tilde{\nu}^*} - \hat{\tau}_{j,\tilde{\nu}^*}) \qquad (6)$$

$\hat{R}_{\tilde{\nu}^*}^{/}$ is a small atmospheric contribution from the surface to the first layer above the surface L. Note that in deriving eq. (5) we implicitly assume that the total transmittance of an atmospheric path is the product of the transmittances of the constituent sub-paths. Although this is true for monochromatic radiation it can be considered a good approximation when the transmittance varies relatively slowly with wavenumber (note that the IASI ISRF is narrow and is essentially symmetric about its centroid). The scene temperature T_j is defined here as the layer mean temperature obtained using the Curtis-Godson air density weighted mean value assuming that the temperature varies linearly between the layer boundaries. The calculation of the sea surface emissivity $\varepsilon_{s,\tilde{\nu}^*}(\theta)$ is performed using the model of Masuda et al.[10]. The refractive index of pure water based on Hale and Querry[11] is adjusted (Friedman[12]) to the sea water value and then interpolated to the wavenumber $\tilde{\nu}^*$ to be given as an input with surface wind speed and the zenith angle θ to compute the rough sea surface emissivity. Figure 1 shows the range spanned by $\varepsilon_{s,\tilde{\nu}^*}(\theta)$ for a number of different scenarios assuming an average wind speed of 7 m s^{-1}. Over land the emissivity is set to 0.97. The top of atmosphere overcast cloudy radiance in discrete notation is defined as:

$$\hat{R}_{\tilde{\nu}^*}^{cld} = \hat{\tau}_{cld,\tilde{\nu}^*}\, B_{\tilde{\nu}^*}(T_{cld}) + \hat{R}_{\tilde{\nu}^*}^{"} + \sum_{j=1}^{L_{cl}} \hat{R}_{j,\tilde{\nu}^*}^{u} \qquad (7)$$

where L_{cl} is the layer above the cloud top and there is an interpolation of the radiance from the level below the cloud top and the level above the cloud top denoted by $\hat{R}_{\tilde{\nu}^*}^{"}$ to provide the additional radiance from the last full layer to the cloud top. Finally an empirical correction to the transmittance is possible by raising the computed transmittance to the power γ where γ is determined empirically. In this paper γ is set equal to 1. The validity of eq (5) was tested by comparing the convolved monochromatic radiances (at a resolution of 0.001 cm^{-1}) with the radiances computed from the convolved transmittances. These exact and approximate convolved radiances were computed for a set of 34 atmospheric profiles (see below) and compared. The differences were typically less than 0.12 K. Since the error introduced by this "polychromatic" approximation is less than the radiometric noise it was considered to be adequate for our purposes.

For a given input atmospheric profile (temperature, water vapour and ozone volume mixing ratio) and surface variables (emissivity, pressure, temperature, skin temperature) the computation of the convolved level-to-space transmittance $\hat{\tau}_{j,\tilde{\nu}^*}$ or convolved level-to-space optical depth $\hat{d}_{j,\tilde{\nu}^*}$ ($\hat{\tau}_{j,\tilde{\nu}^*} = \exp-[\hat{d}_{j,\tilde{\nu}^*}]$) is performed by the fast transmittance model and is the essence of RTIASI. In this paper we assume that the RT equation is integrated on the same levels as the transmittance computation although in principle this is not necessary . The atmosphere is divided into 42 layers whose boundaries are the fixed pressure levels listed in 1. As some IASI channels show absorption features even for very low values of pressure, transmittances are computed also for an additional layer between 0.1 and 0.005 hPa. The number of levels is a compromise between the computing resources and the need to keep the RT errors below the instrument noise. To quantify the errors that are introduced by limiting the number of layers to 43, spectra were computed for two very different atmospheric profiles by dividing the atmosphere into 98 layers. The difference between the two convolved spectra was found to be less than 0.05 K in band 1, less than 0.08 K in band 2 and less than 0.15 K in band 3, all these figures being significantly lower than the instrument noise. As the troposphere and lower stratosphere is the most important region for IASI, the thickness of the layers were selected in that region to be less or at least equal to the nominal IASI 1 km vertical resolution. As shown in table 1, the thickness of the layers varies smoothly with pressure to avoid large changes in layer optical depths and to ease interpolation (either within the line-by-line computations or if the RT equation is integrated on another set of levels); care has also been taken in selecting an adequate number of levels around the tropopause and the boundary layer.

The fast transmittance stage of RTIASI is based on algorithms that have been developed over the years for a number of different satellite instruments (McMillin and Fleming[13]; Fleming and McMillin[14]; McMillin et al.[15]; Susskind et al.[16]; Eyre and Woolf[17]; Eyre[8]; Rayer[18] ; Hannon et al.[19]). In the RTIASI fast transmittance model the computation of the optical depth for the layer from pressure level j to space along a path at angle θ involves a polynomial with terms that are functions of temperature, absorber amount, pressure and viewing angle. The convolved optical depth at wavenumber $\tilde{\nu}^*$ from level j to space can be written as:

$$\hat{d}_{j,\tilde{\nu}^*} = \hat{d}_{j-1,\tilde{\nu}^*} + \sum_{k=1}^{M} a_{j,\tilde{\nu}^*,k} X_{k,j} \qquad (8)$$

where M is the number of predictors and the functions $X_{k,j}$ constitute the profile dependent predictors of the fast transmittance model. To compute the expansion coefficients $a_{j,\tilde{\nu}^*,k}$ (sometimes referred to as fast transmittance coefficients) a set of diverse atmospheric profiles is used to compute, for each profile and for several viewing angles, accurate line-by-line level-to-space transmittances for each level defined by the atmospheric pressure layer grid. The convolved level-to-space transmittances $\hat{\tau}_{j,\tilde{\nu}^*}$ are then used to compute the $a_{j,\tilde{\nu}^*,k}$ coefficients by linear regression of $\hat{d}_{j,\tilde{\nu}^*} - \hat{d}_{j-1,\tilde{\nu}^*}$ (or $-\ln[\hat{\tau}_{j,\tilde{\nu}^*} / \hat{\tau}_{j-1,\tilde{\nu}^*}]$) against the predictor values $X_{k,j}$ calculated from the profile variables for each profile at each of the viewing angles. Note that the regression is made on the layer optical depths rather than on the level-to-space transmittances themselves, as this gives significantly more accurate results (Eyre and Woolf [17]).

3. THE DIVERSE PROFILE DATA SET

For each gas allowed to vary the profiles used to compute the database of line-by-line transmittances are chosen to represent the range of variations in temperature and absorber amount found in the real atmosphere. Only a few atmospheric gases are allowed to vary, the others are held constant and will be referred to as Afixed≅. Gases are considered as fixed if their spatial and temporal concentration variations do not contribute significantly to the observed radiances. In this paper only H_2O and O_3 are allowed to vary (although in localised IASI spectral regions gases such as CO, N_2O and CH_4 could also be considered variable) and fast transmittance coefficients are generated for H_2O, O_3 and fixed gases.

As outlined in the previous section, the transmittances computed for the diverse profiles become the data points in the regression. The water vapour and fixed gas fast transmittance coefficients were derived using a training set of 42 profiles selected from the 1761 profile TOVS Initial Guess Retrieval (TIGR) dataset (for more details see Chedin et al.[20]). For the ozone fast transmittance coefficients 33 ozone profiles (selected from a set of 383 profiles from NESDIS supplemented by a few extreme Antarctic profiles) were used (Rizzi [21]). Note that within the regression scheme the global mean of either the 1761 TIGR profiles and the 383 ozone profiles is included to serve as a reference profile. These profiles were selected to cover most of the range of observed temperature, water vapour and ozone behaviour. The determination of the number of profiles was arrived at as a compromise between the computational time needed to build up the database and the need to cover the range of profile behaviour in the regression.

Each profile has data for temperature and absorber amount that cover the whole range of pressure values used in the radiative transfer computations. However, the quality of the radiosonde stratospheric humidity measurements in the TIGR data set is a matter of concern. Within the framework of a regression-based fast RT model, the provision of some kind of variability to the stratospheric water vapour would be desirable. To provide such variability a compilation has been made of 32 diverse HALOE water vapour profiles (Evans [22]) as a subset of the dataset produced by Harries et al.[23], for the stratosphere. The effective vertical resolution of HALOE varies between 3-4 km; six latitude bands are covered. For each of the 42 TIGR water vapour profiles, the specific humidity was extrapolated with a cubic law in pressure from 300 hPa to 100hPa. The 100hPa value is that obtained averaging the values from the HALOE profiles whose latitude band match the TIGR profile latitude band. The averaged HALOE water vapour values for the latitude band have then been used from 100 hPa to 0.005 hPa to add some realistic variability to the stratospheric humidity as shown in figure 2. The TIGR profile temperature values were retained throughout the pressure range and each profile was checked for supersaturation and adjusted if necessary. The same extrapolation and supersaturation check was applied to the water vapour amount values that come with the ozone profiles.

To optimize the fit of the line-by-line optical depths to the curve defined by the predictors used in the regression it would be desirable that at each pressure level the training profiles were distributed as uniformly as possible across the range spanned by the temperature and water vapour/ozone mixing ratio values at that level (the minimum and maximum values for each level shown in table 1). In principle it is important that the profiles should represent the range of variations in temperature and water vapour/ozone mixing ratio found in the atmosphere and that they should also provide at each pressure level a set of input values suitable for the regression to work well. Although

an effort was made to meet this requirement, as figure 3 shows it could only be partially met not because of the poor representativeness of the training profile but because of the intrinsic high variability of the temperature profiles associated with the dry water vapour profiles. An effort to make a well-balanced distribution of the water vapour profiles would in fact result in a distribution of the temperature profiles that would cover the regions around the extreme ends of the range well but with few profiles covering the middle range. Drier profiles are needed because, in general, most of the profiles that account for the temperature behaviour in this range are thermodynamically linked with dry water vapour profiles. The resultant distributions shown in figures 3a and 3b are a balance between the desirable but incompatible aims of having both the water vapour profiles and the temperature profiles evenly distributed across the pressure levels.

4. THE LINE-BY-LINE TRANSMITTANCE DATABASE

The database of line-by-line atmospheric infrared transmittances is calculated using GENLN2 (Edwards[24]), a general purpose line-by-line atmospheric transmittance and radiance model. The line parameters were obtained from the 1996 edition of the High-resolution Transmission (HITRAN) molecular database (Rothman et al.[25])

The Voigt (Armstrong[26]) line shape was adopted for most gases to describe the effects of both pressure and Doppler line broadening. Carbon dioxide line coupling and non-Lorentzian line wing effects were taken into account as the effects caused by line coupling can produce large differences in very localised spectrally narrow regions. A line shape option is incorporated into the GENLN2 model that includes the effect of line coupling and sub-Lorentzian line wings. The available line coupling coefficients (Strow et al.[27]) were used to compute the GENLN2 CO_2 modified line shape (Edwards[24]).

In addition to line-by-line absorption, the continuum absorption of certain molecules was taken into account. In particular, water vapour continuum is important in the infrared spectral region and is responsible for most of the absorption around 4μm and at 8-12μm. In GENLN2 the water vapour continuum absorption is parameterized using the semi-empirical approach by Clough et al.[28,29]. In addition CO_2, N_2 and O_2 continua are also included. CO_2 continuum is calculated using the GENLN2 line shape (Edwards[24]) while the pressure broadened band of N_2 at 2350 cm^{-1} (Clough et al.[30]; Menoux et al.[31]) and that of O_2 at 1550 cm^{-1} (Timofeyev and Tonkov[32]; Rinsland et al.[33]) are included as broadband continuum contributions to the absorption. Finally to model the heavy molecules (e.g. CFC11 and CFC12) high resolution cross-section data are used.

As stated in section 3, water vapour and ozone are regarded as variable gases. In this paper fixed gases are defined as CO_2, N_2O, CO, N_2, CH_4, O_2, CFC11 and CFC12 and are not profile variables in the fast RT model. For all these constituents tropospheric climatological concentration values for the year 2005 are used following the recommendations of the Intergovernmental Panel On Climate Change (Schimel et al.[34]).

The GENLN2 spectra were computed from 600 cm^{-1} to 3000 cm^{-1} at wavenumbers determined by a fixed wavenumber grid whose spacing defines the resolution of the calculation. Calculations were not performed for extremely weak lines. The resolution used in the GENLN2 spectral computation was determined by studying how the point spacing of the full resolution spectra affected the convolved radiance. The full resolution spectrum is the spectrum convolved with the ISRF in order to generate a simulated spectrum that can be compared to the

observed spectrum. The simplest procedure to generate the full resolution spectra would be to choose a wavenumber grid fine enough that the narrowest line is adequately sampled. This suggests a resolution as high as 0.0005 cm^{-1} which for this work was not practical in terms of available computing resources. As the features of the convolved spectrum are controlled by the spacing of the monochromatic spectrum we decided to arrive at the definition of full resolution spectrum by studying how varying the spacing of the wavenumber grid changed the convolved IASI spectra. Two atmospheric profiles at either end of profile extremes were selected and monochromatic radiance spectra at the top of the atmosphere were computed at an increasingly higher resolution (i.e. S_1, 0.05 cm^{-1}; S_2, 0.005 cm^{-1}; S_3, 0.0025 cm^{-1}; S_4, 0.001 cm^{-1}; S_5, 0.0005 cm^{-1}). The spectra were then convolved and for each profile we compared the IASI radiometric noise figure with the spectra drawn from the differences S_1-S_2, S_2-S_3, S_3-S_4 and S_4-S_5. The greatest differences were found to occur in the strong 15 μm CO_2 absorption band for the extreme tropical profile. Over the IASI wavenumber range only S_4-S_5 was found to be well below the instrument noise. This means that the extra features introduced in the convolved spectra by increasing the wavenumber grid spacing from 0.001 cm^{-1} to 0.0005 cm^{-1} are so small that the instrument cannot detect them. Hence 0.001 cm^{-1} is a sufficient resolution for IASI simulations.

The diverse profile data sets described in section 3 have been used to build the database of line-by-line transmittances required to compute the regression coefficients used by the RTIASI fast transmittance model. Transmittances were computed from 0.005 hPa to each of the 43 standard pressure levels, at 0.001 cm^{-1} resolution, for each atmospheric profile and six scan angles, namely the angles for which the secant has equally spaced values from 1 to 2.25. The transmittance calculations (and the subsequent convolution) represented a massive undertaking, the size of the final database being nearly 500 Gigabytes. The convolved line-by-line transmittances were used to compute three sets of regression coefficients as the fast transmittance model treats separately the absorption by the fixed gases, water vapour and ozone (Eyre [8]). For each term the level-to-space transmittances are computed using an algorithm of the same form as eq. 8, the predictors $X_{k,j}$ (defined in the next section) depending upon the gas. However usually for real, non-monochromatic channels the convolution of the transmittance of all the gases is different from the product of the transmittance of the single gases convolved individually and the monochromatic transmittance approximation

$$\hat{\tau}^{T}_{\tilde{\nu}^*,j} = \hat{\tau}^{F}_{\tilde{\nu}^*,j}\,\hat{\tau}^{WV}_{\tilde{\nu}^*,j}\,\hat{\tau}^{O}_{\tilde{\nu}^*,j} \qquad (9)$$

(where $\hat{\tau}^{T}_{\tilde{\nu}^*,j}$ is the convolved transmittance of all the gases and $\hat{\tau}^{M}_{\tilde{\nu}^*j}$, $\hat{\tau}^{WV}_{\tilde{\nu}^*,j}$, and $\hat{\tau}^{O}_{\tilde{\nu}^*,j}$ are the transmittances of the single gases convolved individually) may not be accurate because for instance absorption by water vapour is not totally uncorrelated with absorption by the fixed gases. Even for the narrow IASI channels the convolved transmittance computed using eq.9 differs significantly from the convolution of the transmittance of all the gases. The line-by-line transmittances from the absorbing gas alone were convolved and compared with the convolved line-by-line transmittance from all the gases for the ozone reference profile. The difference between the correct total transmittance and that computed using eq.9 was found to vary with wavenumber and with level and, for instance, for some of the channels in the 10 μm window region the brightness temperatures computed using the correct transmittances may differ from those computed using eq.9 by ≈0.7 K. To reduce the errors introduced by separating the gas transmittances after the convolution, the monochromatic transmittances were calculated and

grouped in four sets. The water vapour profiles were used to compute one set of level-to-space transmittances for the combined effect of the fixed gases, $\hat{\tau}^{F}_{\tilde{\nu}^*,j}$, and one set for the fixed gases plus water vapour, $\hat{\tau}^{F+WV}_{\tilde{\nu}^*,j}$, whereas the ozone profiles were used to compute one set of level-to-space transmittances for the fixed gases plus water vapour $\hat{\tau}^{(F+WV)'}_{\tilde{\nu}^*,j}$, and one set for the fixed gases plus water vapour and ozone, $\hat{\tau}^{(F+WV+OZ)'}_{\tilde{\nu}^*,j}$ where / over the symbol denotes transmittances from ozone profiles.

The monochromatic transmittances were convolved and used to compute the fixed gases, water vapour and ozone layer optical depths defined as:

$$\hat{d}^{F}_{\tilde{\nu}^*,j} - \hat{d}^{F}_{\tilde{\nu}^*,j-1} = -\ln(\hat{\tau}^{F}_{\tilde{\nu}^*,j} / \hat{\tau}^{F}_{\tilde{\nu}^*,j-1}) \tag{10}$$

$$\hat{d}^{WV}_{\tilde{\nu}^*,j} - \hat{d}^{WV}_{\tilde{\nu}^*,j-1} = -\ln\{[\hat{\tau}^{(F+WV)}_{\tilde{\nu}^*,j} / \hat{\tau}^{(F)}_{\tilde{\nu}^*,j}] \times [\hat{\tau}^{(F)}_{\tilde{\nu}^*,j-1} / \hat{\tau}^{(F+WV)}_{\tilde{\nu}^*,j-1}]\} \tag{11}$$

$$\hat{d}^{O}_{\tilde{\nu}^*,j} - \hat{d}^{O}_{\tilde{\nu}^*,j-1} = -\ln\{[\hat{\tau}^{(F+WV+O)'}_{\tilde{\nu}^*,j} / \hat{\tau}^{(F+WV)'}_{\tilde{\nu}^*,j}] \times [\hat{\tau}^{(F+WV)'}_{\tilde{\nu}^*,j-1} / \hat{\tau}^{(F+WV+O)'}_{\tilde{\nu}^*,j-1}]\} \tag{12}$$

where the transmittance from 0.05 hPa to space (when j-1=0) is set equal to 1. Note that the layer optical depths defined by eq.11 and 12 do not involve any calculation based on absorption of water vapour and ozone alone. These layer optical depths are the data points used in the regression to generate the fixed gases, water vapour and ozone fast transmittance coefficients and are used to compute the model transmittances $\hat{\tau}^{F_{model}}_{\tilde{\nu}^*,j}$, $\hat{\tau}^{WV_{model}}_{\tilde{\nu}^*,j}$ and $\hat{\tau}^{O_{model}}_{\tilde{\nu}^*,j}$ by a polynomial expansion of the same form as eq.(8). The total model transmittance can now be written as:

$$\hat{\tau}^{T_{model}}_{\tilde{\nu}^*,j} = \hat{\tau}^{F_{model}}_{\tilde{\nu}^*,j} \hat{\tau}^{WV_{model}}_{\tilde{\nu}^*,j} \hat{\tau}^{O_{model}}_{\tilde{\nu}^*,j} \tag{13}$$

5. THE FAST TRANSMITTANCE MODEL

The fast model simulates IASI level 1C radiances, which is the radiance product that will be distributed to the NWP centres. To simulate the level 1C radiance the monochromatic Ainfinite resolution≅ spectra must be convolved with an ISRF defined as the convolution of a 0.5 cm^{-1} Full Width Half Height (FWHH) Gaussian with a cardinal sinc function whose interferogram is a ± 2 cm box function (Cayla[35]). The spectra were convolved applying to eq. (4) the convolution theorem (Brigham[36]). The Fast Fourier Transform (FFT) of the transmittance spectra were multiplied by the FFT of the Gaussian and the interferograms obtained were truncated corresponding to the IASI ±2 cm optical path; the convolved spectra were then recovered by performing the Inverse Fast Fourier Transform of the truncated interferogram.

The truncation of the interferogram at ±2 cm and the errors introduced by the FFT routine were found to cause the occurrence of fixed gases and water vapour negative convolved transmittances in the strong absorption bands centred at 15 μm, CO_2, 6.3μm, H_2O and 4.3 μm, CO_2 and N_2O. The general trend is that of a transmittance that

becomes negative when the transmittance above the layer is typically less than 10^{-4}. As the occurrence of negative transmittances does not allow Lambert's law ($\tau = \exp[-d]$) to be satisfied we shifted all the transmittances by a constant offset such that positive values were always obtained. These modified transmittances were then used to compute the layer modified optical depths that become the data points in the regression. For level *j* the (positive or negative) level-to-space transmittance $\hat{\tau}_{\tilde{\nu}^*,j}$ can then be recovered as

$$\hat{\tau}_{\tilde{\nu}^*,j} = \hat{\tau}_{\tilde{\nu}^*,j-1}\{\exp[-(\hat{d}'_{\tilde{\nu}^*,j} - \hat{d}'_{\tilde{\nu}^*,j-1})] + \exp[-(\hat{d}'_{\tilde{\nu}^*,j} - \hat{d}'_{\tilde{\nu}^*,j-1})](C/\hat{\tau}_{\tilde{\nu}^*,j-1}) - (C/\hat{\tau}_{\tilde{\nu}^*,j-1})\} \qquad (14)$$

where $\hat{d}'_{\tilde{\nu}^*,j} - \hat{d}'_{\tilde{\nu}^*,j-1}$ is the modified layer optical depth and C is the offset constant taken as 0.06. Note that over the layers where the negative transmittances occur, the total transmittance has already become small enough that the contribution of these layers to the radiance is negligible.

The functional dependence of the predictors $X_{j,k}$ used to parameterize the optical depth $\hat{d}'_{\tilde{\nu}^*,j}$ depends mainly on factors such as the absorbing gas, ISRF and spectral region although also the order in which the gases are separated out (eq. 11 and eq.12) and the layer thickness can be important. The predictors $X_{j,k}$ used in this paper are based, with modifications, on those selected for the Atmospheric Infrared Sounder (AIRS) fast transmittance model (Hannon et al. [19]; Strow [37]) since most of the problems posed by finding an optimal set of predictors that work well for the thousands of channels of an instrument such as AIRS were also expected to be encountered for an instrument such as IASI with its 8461 channels. The most basic predictors (all defined in table 3) are defined from the ratios $T_r(j)$, $W_r(j)$, $O_r(j)$ and from the differences $\delta T(j)$. This is because within the framework of a linear regression method the great variability between extreme profiles makes the regression prone to numerical instabilities and thus difficulties in calculating the coefficients can arise if the predictors are allowed to vary too much. Simple functions involving combinations of the basic predictors and of the viewing angle can account for the behaviour of the layer optical depth of a gas treated as having the transmittance properties of a gas in a homogeneous layer at pressure *P*, temperature *T* and absorber amount *n*. This can be accurate for monochromatic transmittances but in practice we have to predict polychromatic transmittances and additional terms based on those given by McMillin and Fleming[14] are added. These are the predictors $T_w(l)$, $W_w(l)$, $O_w(l)$. These predictors account for the dependence of the layer transmittance on the properties of the atmosphere above the layer. Note that although the use of equations (9), (10) and (11) reduces this dependence, nevertheless, for a temperature sounding channel the layer transmittance for two profiles having the same mean layer temperature but different temperature profiles over the actual layer will still differ in that the profile with greater optical depth above the layer will have a smaller optical depth within the layer.

The final form of the IASI predictors was defined carrying out trials in which some changes were made to the AIRS fast transmittance model predictors (Hannon et al. [19]; Strow [37]). As for the AIRS predictors the precise form of the terms used in the parameterization was arrived at empirically. A representative variation of the layer optical depth with layer temperature, water vapour layer amount and ozone layer amount is shown in figures 4a, 4b and 4c where a temperature sounding channel, a water vapour sounding channel and an ozone sounding channel are selected. In particular figure 4b shows a typical behaviour encountered in many strong water vapour channels, i.e

an abrupt change in the behaviour of the layer optical depth takes place when the attenuation in the atmosphere above the layer is strong. This pattern is difficult to model and it was found that the most sensible approach was to split the water vapour algorithm in two: one where $\hat{d}^{T'}_{\tilde{\nu}^*,j} W_w(j) < 2$ ($\hat{d}^{T'}_{\tilde{\nu}^*,j}$ is the total modified optical depth above layer j) and one where $\hat{d}^{T'}_{\tilde{\nu}^*,j} W_w(j) > 2$. In the first case the data points used in the regression are the layer modified optical depths that lie broadly on the main curve, in the second case the points are those that broadly branch off the main curve. In both cases the functional dependence of the predictors was kept the same. Note that the use of a split algorithm means that a running sum must be maintained in the fast transmittance model in order to use the appropriate regression coefficients. The model predictors for fixed gases, water vapour and ozone are listed in table 2 while the profile variables are defined in table 3.

6. FAST MODEL COMPARISON WITH LINE-BY-LINE MODEL TRANSMITTANCES

The fast model accuracy can be assessed by comparing with the original line-by-line model transmittances and top of atmosphere radiances. The former is more useful to understand how the model performs and see where it needs to be improved, but the latter is the most important as the radiances are what will be used. Both assessements are described below.

For transmittance the fast model simulations were checked by comparing $\hat{\tau}^{F+WV}_{\tilde{\nu}^*,j}$ with $\hat{\tau}^{F\,model}_{\tilde{\nu}^*,j}$ $\hat{\tau}^{WV\,model}_{\tilde{\nu}^*,j}$ and $\hat{\tau}^{(O)'}_{\tilde{\nu}^*,j}$ with $\hat{\tau}^{O\,model}_{\tilde{\nu}^*,j}$. The line-by-line transmittances were subtracted from the fast model transmittance and the root mean square (rms) of the differences $\hat{\tau}^{F+W}_{\tilde{\nu}^*,j} - \hat{\tau}^{F\,model}_{\tilde{\nu}^*,j}$ $\hat{\tau}^{WV\,model}_{\tilde{\nu}^*,j}$ and $\hat{\tau}^{(O)'}_{\tilde{\nu}^*,j} - \hat{\tau}^{O\,model}_{\tilde{\nu}^*,j}$ was calculated at each pressure level using the data provided for each of the profiles used to compute the water vapour/mixed gases and ozone regression coefficients at the 6 viewing angles. In IASI band 1 the radiances originate mainly from CO_2 and O_3 with water vapour continuum responsible for most of the emission/absorption in the 8-12 μm region. For the channels for which CO_2 is the dominant contributor the maximum value of the rms in transmittance ranges between 0.0005 and 0.006 whereas in the infrared "window" region the rms is less than 0.005. In the region where ozone is the dominant contributor the maximum value of the rms peaks at 0.007. Band 2 is largerly dominated by water vapour absorption with some contribution from N_2O and CH_4. In the region where N_2O and CH_4 contribute to the absorption, the maximum value of the rms ranges between 0.0003 and 0.005, elsewhere the rms can be as high as 0.013. Fixed gases (CO, N_2O and CO_2) are the dominant contributors in band 3 with water vapour and ozone also contributing to the line and continuum (water vapour) absorption. In the region where ozone and water vapour line absorption is present, the rms ranges between 0.0005 and 0.007, elsewhere the rms can be as small as 0.0002 and never greater than 0.003.

The error in computing brightness temperatures that arise from using the fast model transmittances in eq. (5) was calculated with respect to the regression profiles by comparing the brightness temperatures computed using the line-by-line transmittances with those computed using the fast model transmittances. The surface emissivity at each of the six viewing angles was fully accounted for assuming an average wind speed of 7 m s^{-1} and the surface temperature was set equal to the 1013.25 hPa air temperature. Errors were computed for ozone alone and for fixed gases plus water vapour. Figures 5a and 5b show the ability of the fast transmittance model to reproduce the

brightness temperatures for the profiles used to compute the regression coefficients. Figure 5a summarizes the rms error in brightness temperature for the 43 profiles by using $\hat{\tau}^{F+WV}_{\tilde{\nu}^*,j}$ compared with $\hat{\tau}^{F\ model}_{\tilde{\nu}^*,j}\ \hat{\tau}^{WV\ model}_{\tilde{\nu}^*,j}$ while figure 5b summarizes the rms error in brightness temperature for the 34 profiles by using $\hat{\tau}^{(F+WV+O)'}_{\tilde{\nu}^*,j}$ compared with $\hat{\tau}^{(F+W)'}_{\tilde{\nu}^*,j}\ \hat{\tau}^{(O)\ model}_{\tilde{\nu}^*,j}$. The largest source of error comes from the water vapour and the ozone model but in general the transmittance model fits the regression profiles very well, the rms errors being at or below the instrument noise except for some ozone channels where a further tuning of the predictors appears necessary to reduce the errors below the noise. The skill of the fast transmittance scheme has also been tested using the water vapour and temperature profiles that come with the 34 ozone profiles to test the ability of the fast model to reproduce the water vapour and fixed gases line-by-line transmittances for a set of profiles that are independent of the regression coefficients. Figure 5c shows the rms of the error in brightness temperature for the 34 profiles by using $\hat{\tau}^{(F+WV+O)'}_{\tilde{\nu}^*,j}$ compared with $\hat{\tau}^{F\ model}_{\tilde{\nu}^*,j}\ \hat{\tau}^{WV\ model}_{\tilde{\nu}^*,j}\ \hat{\tau}^{O\ model}_{\tilde{\nu}^*,j}$ (note that these profiles are the dependent set for the ozone regression coefficients). The most noticeable feature is an increase of the error for the strong water vapour channels in IASI band 2. For these channels the worst errors are in general found for very warm moist tropical atmospheres. The set of 34 ozone profiles contains a large and disproportionate number of such profiles and so yields worst errors for these channels. Tests carried out selecting the independent profiles (among the 34) for other latitude bands show that the errors are reduced significantly. Note that spectroscopic errors in the line-by-line models are not addressed here. Recent work on the (A)TOVS fast model (Saunders et al.[5]) has shown the uncertainties in the spectroscopy for some channels are much larger than the fast model errors.

7. CONCLUSIONS

The forthcoming launch of IASI, with a much higher spectral resolution than the existing HIRS radiometer, offers the exciting possibility of a significant improvement in the vertical resolution of profiles of temperature and constituents for use in numerical weather prediction. The objective of this study was to develop a fast radiative transfer model for IASI in preparation for exploitation of the IASI data in an NWP model using a variational analysis scheme. The model fit to the line-by-line radiances shows that the fast model can reproduce the line-by-line transmittances to a degree of accuracy that for most of the channels is at or below the instrumental noise. The degree of accuracy is considered to be adequate for operational use in NWP data assimilation and for most of the channels will not add significantly to the errors that are likely to be introduced in the line-by-line model by inaccuracies in the spectroscopic data. For most of the temperature sounding channels the error is largely independent of the nature of the input atmosphere (warm/moist and cold/dry atmospheres are expected to be modelled to very much the same degree of accuracy) whereas the performance for the strong water vapour channels depends on whether or not the atmosphere is a warm/moist or a cold/dry one (the former yields the larger errors). A fine tuning of the predictors is required to improve the skill of the fast transmittance scheme for the strong water vapour channels in IASI band 2 (above all when modelling warm moist atmospheres) and in the strong 9.8 μm ozone band.

Although the performance of RTIASI is considered adequate for this study some improvements could be made as we move towards the launch of IASI.

The fast model developed for this study allows a set of IASI radiances to be computed using a given profile of temperature and constituent concentrations. In order to assimilate IASI radiances in a variational assimilation scheme the gradient computations also have to be made and for this purpose RTIASI gradient routines are currently under development.

Any improvement in spectroscopic line databases and line-shape formulations should be included in the fast model coefficients (the former appears to be the major source of error in the forward calculations). The treatment of the water vapour continuum should account for the most recent developments in this field as well as the treatment of the CO_2 line mixing for which new coefficients are available.

A revision of the minor constituents profiles (fixed gases) should be considered to mirror better the state of the actual/future atmosphere. In this respect some fixed gases could be allowed to vary using a parameterisation of the same type as that used for the variable gases.

Finally, for the shorter wavelenghts a solar contribution term could be added to the simulated radiance and the treatment of the reflected thermal term in the radiative transfer equation could be improved from the current approximate formulation.

Acknowledgements

This work was supported by EUMETSAT contract EUM/CO/96/389/DD. Many individuals have contributed to this study. We wish to acknowledge particularly the useful discussions with R. Rizzi, Universita' di Bologna, L. Strow, University of Maryland, P. Rayer, U.K. Met. Office, F. Cayla, CNES and S.J. Evans, Imperial College.

REFERENCES

э European Organisation for the exploitation of Meteorological Satellites.

H Television Infra-Red Observation Satellite.

1. GEWEX Science Plan, WMO document WMO/TD No. 376 (Geneva, 1990).

2. W.L. Smith, H.M. Woolf, C.M. Hayden, D.Q. Mark and L.M. McMillin, AThe TIROS-N Operational Vertical Sounder,≅ Bull. Am. Meteorol. Soc., **60**, 1177-1187 (1979).

3. J.R. Eyre, G.A. Kelly, A.P. McNally, E. Anderson and A. Persson, "Assimilation of TOVS radiance information through one-dimensional variational analysis," Q.J.Royal Meteorological Society **119**, 1427-1463 (1993).

4. F. Rabier, J. Thépaut and P. Courtier, "Extended assimilation and forecast experiments with a four dimensional variational assimilation system," Q.J.Royal Meteorological Society **124**, 1861-1887 (1998).

5. R. Saunders, M. Matricardi and P. Brunel, "An improved fast radiative transfer model for assimilation of satellite radiance observations," Q.J.Royal Meteorological Society **125**, 1407-1425 (1999).

6. L.M. McMillin, L.J. Crone, M.D. Goldberg and T.J. Kleespies, "Atmospheric transmittances of an absorbing gas 4," Applied Optics **34**, 6269-6274 (1995).

7. L.M. McMillin, L.J. Crone and T.J. Kleespies, "Atmospheric transmittance of an absorbing gas 5," Applied Optics **34**, 8396-8399 (1995).

8. J.R. Eyre, "A fast radiative transfer model for satellite sounding systems, " ECMWF Research Department Technical Memorandum 176 (European Centre for Medium-Range Weather Forecasts, Reading, 1991).

9. R.M. Goody and Y.L. Yung, AAtmospheric Radiation. Theoretical Basis,≅ (Oxford University Press, Inc., New York, 1995).

10. K. Masuda, T. Takashima and T. Takayama, "Emissivity of pure sea waters for the model sea surface in the infrared window regions," Remote sensing of environment **24**, 313-329 (1988).

11. G.M. Hale and M.R. Querry, "Optical constants of water in the 200-nm to 200-μm wavelength region," Applied Optics **12**, 555-563 (1973).

12. D. Friedman, "Infrared characteristics of ocean water (1.5-15 μm).,"Applied Optics **8**, 2073-2078 (1969).

13. L.M. McMillin and H.E. Fleming, "Atmospheric transmittance of an absorbing gas: a computationally fast and accurate transmittance model for absorbing gases with constant mixing ratios in inhomogeneous atmospheres," Applied optics **15**, 358-363 (1976).

14. H.E. Fleming and L.M. McMillin, "Atmospheric transmittance of an absorbing gas. 2. A computationally fast and accurate transmittance model for slant paths at different zenith angles," Applied optics **16**, 1366-1370 (1977).

15. L.M. McMillin, H.F. Fleming and M.L. Hill, " Atmospheric transmittances of an absorbing gas 3," Applied Optics **18**, 1600-1606 (1979).

16. J. Susskind, J. Rosenfeld and D. Reuter, "An accurate radiative transfer model for use in the direct physical inversion of HIRS2 and MSU temperature sounding data," J. Geophys. Res. **88**, 8550-8568 (1983).

17. J.R. Eyre and H.M. Woolf, "Transmittance of atmospheric gases in the microwave region: a fast model," Applied Optics **27**, 3244-3249 (1988).

18. P.J. Rayer, "Fast transmittance model for satellite sounding," Applied Optics **34**, 7387-7394 (1995).

19. S. Hannon., L. Strow and W.W. McMillan, "Atmospheric Infrared Fast Transmittance Models: A comparison of Two Approaches," in *Proceedings of SPIE Conference on Optical Spectroscopic Techniques and Instrumentation for Atmospheric and Space Research 2*, 1996.

20. A. Chedin, N.A. Scott, C. Wahiche and P. Moulnier, "The improved initialization inversion method: a high resolution physical method for temperature retrievals from satellites of the TIROS-N series," Journal of climate and applied meteorology **24**, 128-143 (1985).

21. R. Rizzi, Universita= di Bologna, Dipartimento di Fisica (personal communication, 1996).

22. S.J. Evans, Imperial College, London (personal communication, 1997)

23. J.E. Harries, J.M. Russel, A.F. Tuck, L.L. Gordley, P. Purcell, K. Stone, R.M. Bevilacqua, M. Gunson, G. Nedoluha and W.A. Traub, "Validation of measurements of water vapour from the Halogen Occultation Experiment (HALOE)," J. Geophys. Re s. **101**, 10205-10216 (1996).

24. D.P. Edwards, "GENLN2. A general Line-by-Line Atmospheric Transmittance and Radiance Model," NCAR Technical note NCAR/TN-367+STR (National Center for Atmospheric Research, Boulder,Co., 1992).

25. Rothman, L.S., Schroeder, J., Mc Cann, A., Gamache, R.R., Watson, R.B., Flaud, J.M., Perrin, A., Dana, V., Mandin, J.Y., Goldman, A., Massie, S., Varanasi, P. and Yoshino,K., " HAWKS96, The HITRAN Atmospheric Workstation," in *Proceedings of the fourth Conference of Atmospheric Spectroscopy Applications*, Université de Reims Champagne-Ardenne, Reims, 1996.

26. B.H. Armstrong, "Spectrum line profiles: the Voigt function," J. Quant. Spectrosc. Radiat. Transfer **7**, 66-88 (1967).

27. L.L. Strow, D.C Tobin and S.E. Hannon, "A compilation of First-Order Line-Mixing coefficients for CO_2 Q-branches," J. Quant. Spectrosc. Radiat. Transfer **52**, 281-294 (1994).

28. S.A. Clough, F.X. Kneizys, R. Davies, R. Gamache and R. Tipping, "Theoretical line shape for H_2O vapour; Application to the continuum," in *Atmospheric water vapour*, A. Deepack, T.D. Wilkerson and L.H. Ruhnke, eds. (Academic, New York, 1980), pp. 25-46.

29. S.A. Clough, F.X. Kneizys and R.W. Davis, "Line shape and the water vapour continuum," Atmospheric research **23**, 229-241 (1989).

30. S.A. Clough, F.X. Kneizys, L.S. Rothman and W.O. Gallery, "Atmospheric spectral transmission and radiance: FASCOD1B," in *Proceedings of SPIE conference on Atmospheric Transmission*, 152-166, Washington, DC, 1981.

31. V. Menoux, R. Le Doucen, C. Boulet, A. Roblin and A.M. Bouchardy, "Collision induced absorption in the fundamental Band of N_2," Applied Optics **32**. 263-268 (1993).

32. Y.M. Timofeyev and M.V. Tonkov, "Effect of the induced Oxygen absorption band on the transformation of radiation in the 6 μm region of the Earth's atmosphere," Izvestiya, Atmospheric and Ocean Physics **14**, 437-441 (1978).

33. C.P. Rinsland, J.S. Zander, J.S Namkung, C.B. Farmer and R.H. Norton, "Stratospheric infrared continuum absorption observed by the ATMOS instrument," J. Geophys. res. **94**, 16303-16322 (1989).

34. D. Schimel, D. Alves, I. Enting, M. Heiman, F. Joos, D. Raynaud, T. Wigley, M. Prather, R. Derwent, D. Ehalt, P. Fraser, E. Sanhueza, X. Zhou, P. Jonas, R. Charlson, H. Rodhe, S. Sadasivan, K.P. Shine, Y. Fouquart, V. Ramaswamy, S. Solomon, J. Srinivasan, D. Albritton, R. Derwent, I. Isaksen, M. Lal and D. Wuebbles, " Radiative Forcing of Climate Change," in *Climate Change 1995, The Science of Climate Change,* J.T. Houghton, L.G.Meira Filho, B.A. Callander, N. Harris, A. Kattenberg and K. Maskell eds. (Cambridge University Press, Cambridge, U.K., 1996), pp 69-131.

35. F. Cayla, "Simulation of IASI spectra," CNES document IA-TN-0000-5627-CNE (Centre National D' Etudes Spatiales, Toulouse, 1996).

36. E.O. Brigham, "The Fast Fourier Transform," (Prentice-Hall, Inc., Englewood Cliffs, N.J., 1974).

37. L.L. Strow, University of Maryland, Baltimore County (personal communication, 1998).

Level	Pressure (hPa)	Temperature (K)		Water vapour mixing ratio (ppmv)		Ozone mixing ratio (ppmv)	
		Min	Max	Min	Max	Min	Max
1	0.10	190.9450	288.1028	4.3612	5.8673	0.6800	8.9500
2	0.29	215.5050	296.6161	5.4099	6.2339	1.2492	9.2442
3	0.69	212.8999	310.9560	5.6356	6.1755	1.4096	9.3404
4	1.42	198.4644	309.3185	5.4294	6.0463	1.4132	9.3710
5	2.61	198.4496	300.2095	4.8498	5.7410	1.4146	9.3856
6	4.41	204.5798	289.6117	4.6237	5.7031	1.4156	9.3928
7	6.95	189.3978	290.7231	4.2749	5.8440	1.4159	9.3965
8	10.37	186.9405	285.7654	3.9638	5.8308	1.4162	9.4034
9	14.81	185.8896	264.9886	3.7416	5.3690	1.4163	9.4337
10	20.40	186.1667	261.3101	3.6905	5.3979	1.4165	8.8513
11	27.26	183.1527	257.8293	3.5499	5.5928	1.3603	8.7671
12	35.51	183.6486	253.1519	2.9945	4.8522	0.5584	6.2765
13	45.29	184.5035	251.5889	2.7392	4.5938	0.3678	6.0648
14	56.73	183.7715	254.8312	1.9161	4.4561	0.1907	5.3851
15	69.97	186.2423	250.4318	2.4117	4.3336	0.1429	3.5447
16	85.18	185.1949	243.4454	1.6437	4.0254	0.1146	2.9121
17	102.50	186.2353	242.3198	1.6514	3.8896	0.0466	2.2501
18	122.04	189.8716	241.5646	2.5985	47.889	0.0079	1.9913
19	143.84	189.5201	240.8297	2.0776	115.36	0.0069	1.6800
20	167.95	189.3538	242.2247	1.7279	220.16	0.0058	1.2264
21	194.36	191.6970	243.8277	2.2201	373.29	0.0049	0.8982
22	222.94	196.3361	245.8346	3.2017	594.20	0.0048	0.8089
23	253.71	201.8183	253.0286	3.2112	1024.2	0.0080	0.5956
24	286.60	204.3071	253.6444	3.1778	1496.4	0.0078	0.4170
25	321.50	207.7184	259.7492	1.4466	2253.2	0.0107	0.3237
26	358.28	208.7572	266.1804	0.3097	3406.2	0.0053	0.2101
27	396.81	211.7302	271.1689	2.1929	4853.4	0.0075	0.1716
28	436.95	216.1444	273.4873	2.7839	6701.6	0.0044	0.1342
29	478.54	220.3337	274.3341	5.3909	8711.7	0.0042	0.1286
30	521.46	222.7711	275.3654	8.0507	10387	0.0033	0.1265
31	565.54	226.1762	279.0348	8.0507	11990	0.0019	0.1168
32	610.60	230.0194	282.4702	21.168	14121	0.0016	0.1104
33	656.43	233.5735	284.9223	41.511	16615	0.0015	0.1134
34	702.73	235.5786	289.6340	100.79	18891	0.0014	0.1211
35	749.12	236.9657	294.6081	127.08	21266	0.0004	0.1027
36	795.09	237.2966	299.0551	113.42	23771	0.0004	0.1048
37	839.95	235.5742	303.4185	112.63	26735	0.0004	0.0990
38	882.80	234.810	306.0771	142.72	28639	0.0000	0.0946
39	922.46	234.7339	306.4893	134.58	32190	0.0000	0.0922
40	957.44	235.1377	308.8958	135.77	36126	0.0000	0.0902
41	985.88	236.1328	310.5137	148.33	37362	0.0000	0.0894
42	1005.43	233.8223	311.5381	76.346	37787	0.0000	0.0888
43	1013.25	232.2004	311.9639	42.339	38028	0.0000	0.0886

Table 1. The minimum and maximum values of the temperature, water vapour and ozone values used in the regression at each point of the pressure layer grid

Predictor	Fixed gases	Water vapour	Ozone
$X_{j,1}$	$\sec(\theta)$	$\sec(\theta)W_r^2(j)$	$\sec(\theta)O_r(j)$
$X_{j,2}$	$\sec^2(\theta)$	$\sec^2(\theta)W_r^2(j)$	$\sqrt{\sec(\theta)O_r(j)}$
$X_{j,3}$	$\sec(\theta)T_r(j)$	$(\sec(\theta)W_w(j))^2$	$\sec(\theta)O_r(j)\delta T(j)$
$X_{j,4}$	$\sec(\theta)T_r^2(j)$	$(\sec(\theta)W_w(j))^4$	$(\sec(\theta)O_r(j))^2$
$X_{j,5}$	$T_r(j)$	$\sec(\theta)W_r(j)\delta T(j)$	$\sqrt{\sec(\theta)O_r(j)}\ \delta T(j)$
$X_{j,6}$	$T_r^2(j)$	$\sqrt{\sec(\theta)W_r(j)}$	$\sec(\theta)O_r(j)^2 O_{uw}(j)$
$X_{j,7}$	$\sec(\theta)T_w(j)$	$\sqrt[4]{\sec(\theta)W_r(j)}$	$\frac{O_r(j)}{O_{uw}(j)}\sqrt{\sec(\theta)O_r(j)}$
$X_{j,8}$	$\sec(\theta)\frac{T_w(j)}{T_r(j)}$	$\sec(\theta)W_r(j)$	$\sec(\theta)O_r(j)\frac{O_w(j)}{O_{uw}(j)}$
$X_{j,9}$	$\sqrt{\sec(\theta)}$	$(\sec(\theta)W_r(j))^3$	$O_r(j)\sec(\theta)\sqrt{(O_{uw}(j)\sec(\theta)}$
$X_{j,10}$	$\sqrt{\sec(\theta)}\ \sqrt[4]{T_w(j)}$	$W_r(j)$	$\sec^2(\theta)O_r(j)OT_w(j)$
$X_{j,11}$	0.0	$\sec(\theta)W_r(j)\delta T(j)\lvert\delta T(j)\rvert$	0.0
$X_{j,12}$	0.0	$(\sqrt{\sec(\theta)W_r(j)}\ )\delta T(j)$	0.0
$X_{j,13}$	0.0	$\frac{(\sec(\theta)W_r(j))^2}{W_w}$	0.0
$X_{j,14}$	0.0	$\frac{\sqrt{(\sec(\theta)W_r(j)}W_r(j)}{W_w(j)}$	0.0

Table 2. Regression Predictors used by RTIASI for Fixed Gases, Water Vapour and Ozone

$T(l) = [T^{profile}(l+1) + T^{profile}(l)] / 2$ $\quad T^*(l) = [T^{reference}(l+1) + T^{reference}(l)] / 2$

$W(l) = [W^{profile}(l+1) + W^{profile}(l)] / 2$ $\quad W^*(l) = [W^{reference}(l+1) + W^{reference}(l)] / 2$

$O(l) = [O^{profile}(l+1) + O^{profile}(l)] / 2$ $\quad O^*(l) = [O^{reference}(l+1) + O^{reference}(l)] / 2$

$P(l) = [Pres(l+1) + Pres(l)] / 2$

$T_r(l) = T(l) / T^*(l)$ $\quad \delta T(l) = T(l) - T^*(l)$ $\quad W_r(l) = W(l) / W^*(l)$

$O_r(l) = O(l) / O^*(l)$

$T_w(l) = \sum_{i=2}^{l} P(i)[P(i) - P(i-1)] T_r(i-1)$

$W_w(l) = \sum_{i=1}^{l} P(i)[P(i) - P(i-1)] W(i) / \sum_{i=1}^{l} P(i)[P(i) - P(i-1)] W^*(i)$

$O_w(l) = \sum_{i=1}^{l} P(i)[P(i) - P(i-1)] O(i) / \sum_{i=1}^{l} P(i)[P(i) - P(i-1)] O^*(j)$

$O_{uw}(l) = \sum_{i=1}^{l} O(i) / \sum_{i=1}^{l} O^*(j)$

$OT_w(l) = \sum_{i=2}^{l} P(i)[P(i) - P(i-1)] \delta T(i-1) O_r(i-1)$

Table 3. Definition of profile variables used in predictors defined in Table2

The $Pres(l)$'s are the values of the pressure at each level. $T^{profile}(l)$, $W^{profile}(l)$ and $O^{profile}(l)$ are the temperature, water vapour mixing ratio and ozone mixing ratio profiles. $T^{reference}(l)$, $W^{reference}(l)$ and $O^{reference}(l)$ are corresponding reference profiles. For these variables l refers to the lth level; otherwise l is the lth layer, i.e.the layer above the lth level. Note that we take $P(0) = 2P(1) - P(2)$. Also $T_w(1) = 0$ and $OT_w(1) = 0$.

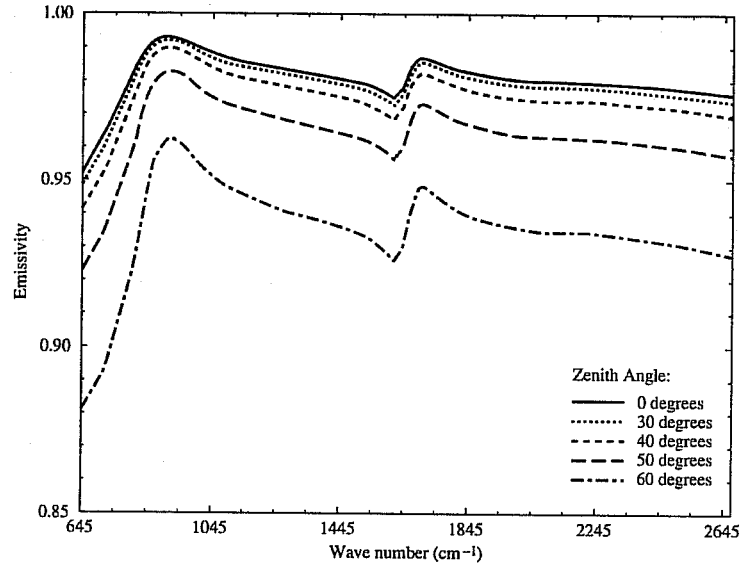

Fig. 1 Computed sea surface emissivity for IASI channels. The wind speed is set to a reference value of 7 m s^{-1}.

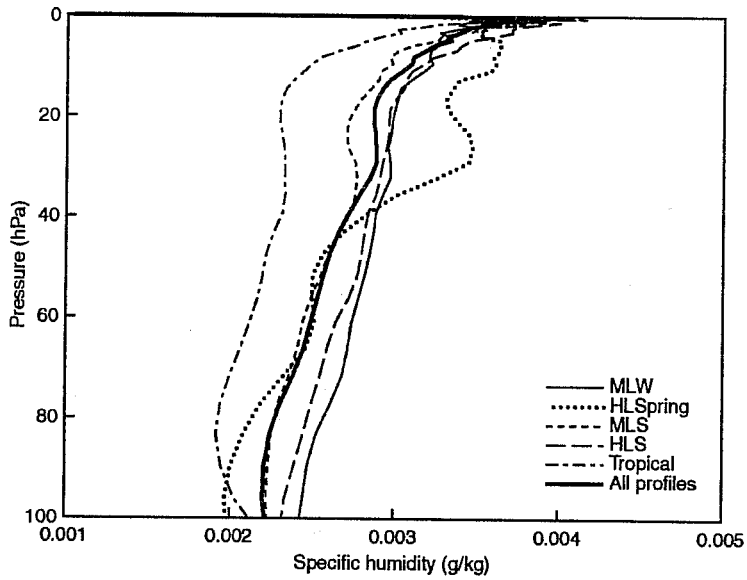

Fig 2 Upper tropospheric/stratospheric water vapour from HALOE measurements. The average profile for each of the latitude bands covered by the 32 profile subset is shown.

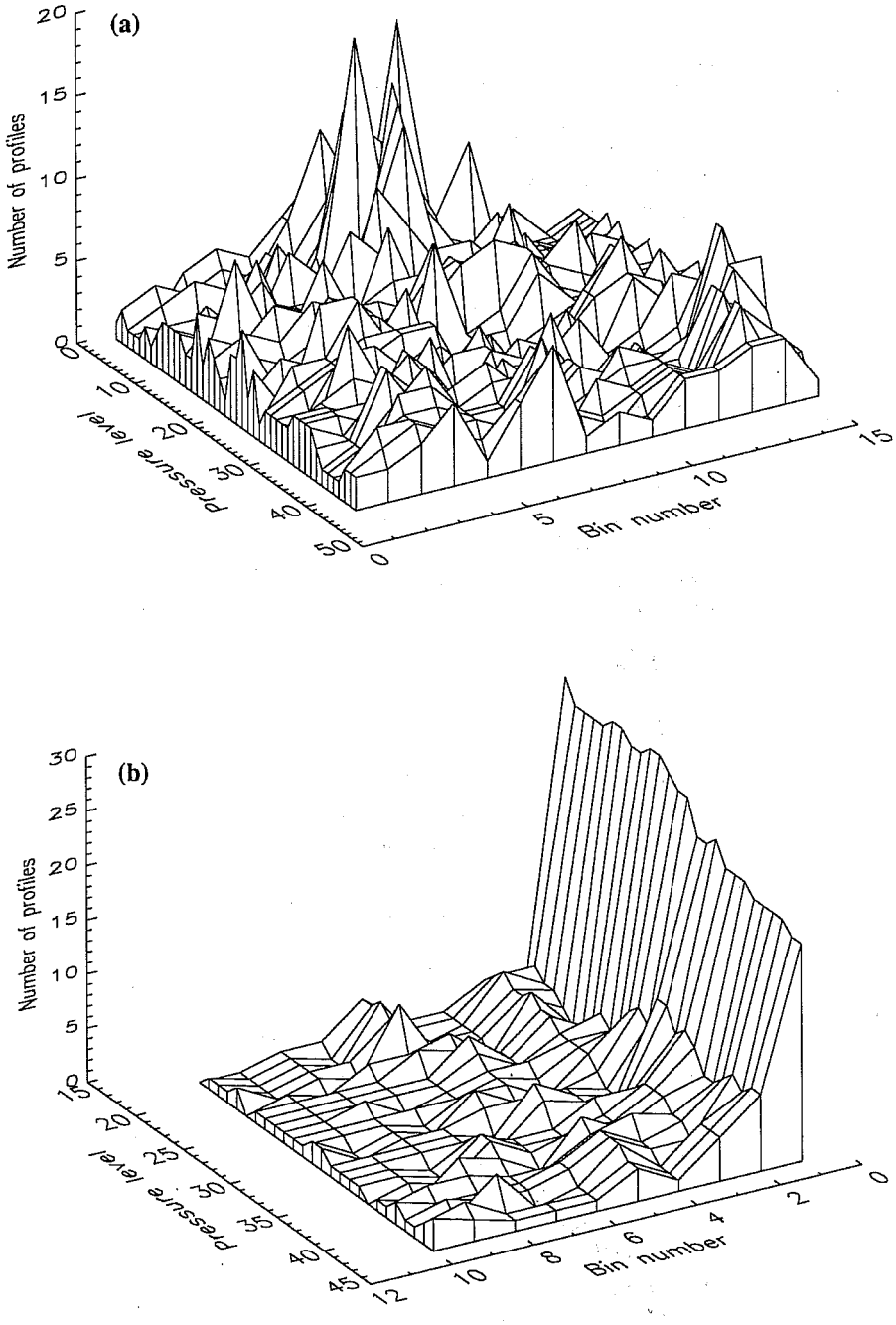

Fig 3 Histogram of frequency by bin number and pressure level for the 43 training profiles. At each pressure level the water vapour mixing ratio and temperature range is divided into a number of bins and the number of training profiles falling within each bin is shown for: (a) water vapour profiles. Pressure values up to 100 hPa are shown; (b) temperature profiles.

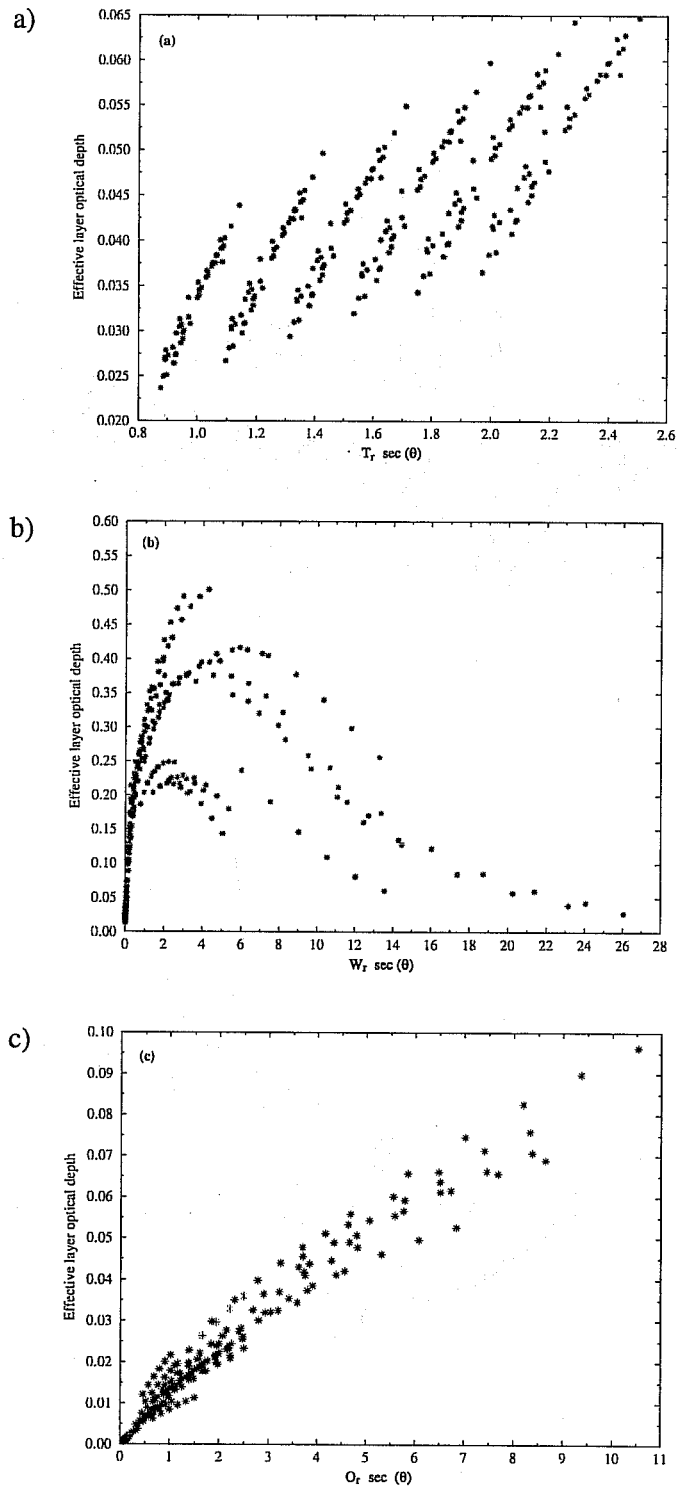

Fig 4 Example of how the layer optical depth varies for: (a) fixed gases at a frequency of 730 cm^{-1} and layer pressures between 102.5 and 85.18 hPa; (b) water vapour at a frequency of 1260.25 cm^{-1} and layer pressures between 521.46 and 478.54 hPa; (c) ozone at a frequency of 1034 cm^{-1} and layer pressures between 253.71 and 222.94 hPa. The ordinates are defined in Table 3.

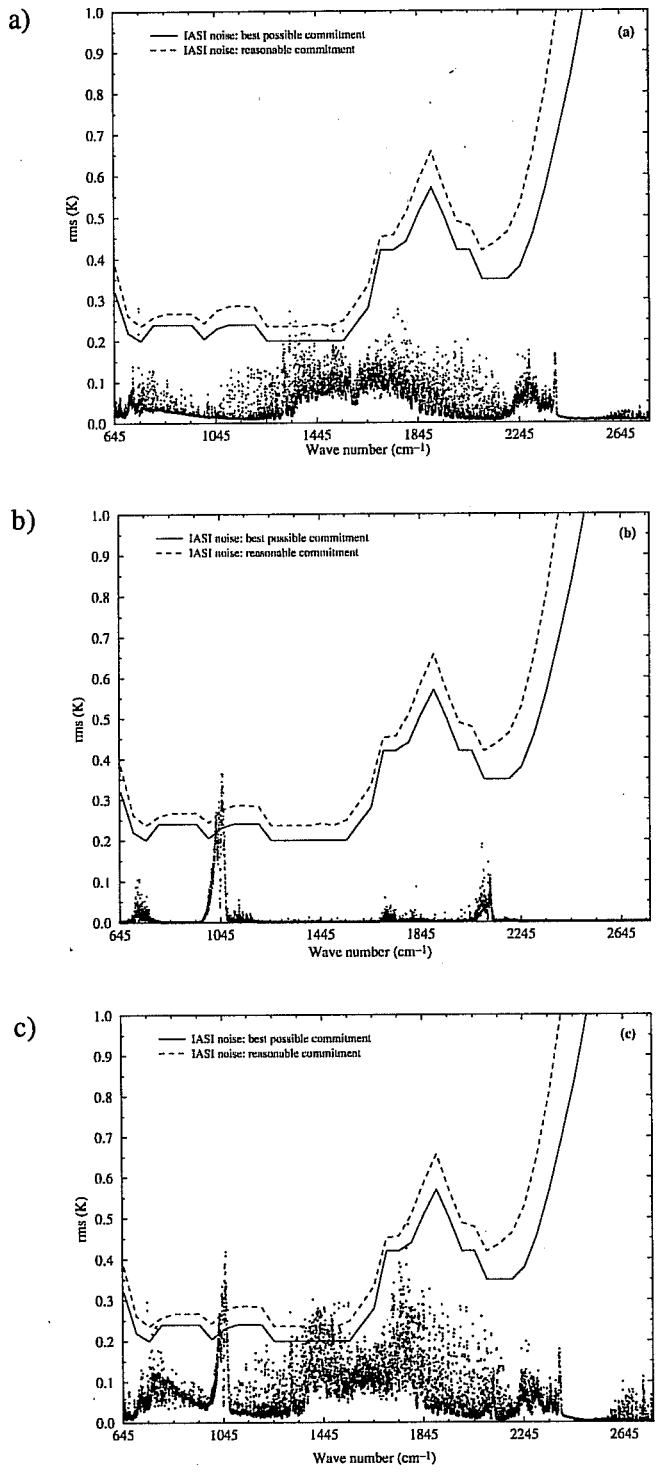

Fig 5 Statistics of the difference between brightness temperatures computed using the fast model and line-by-line transmittances. Root mean square of the error for: (a) water vapour plus fixed gases, the dependent set of profiles for the water vapour and fixed gases regression coefficients is used; (b) ozone, the dependent set of profiles for the ozone regression coefficients is used; (c) water vapour plus fixed gases and ozone for an independent profile set.